THE JOURNAL OF BIOLOGICAL CHEMISTRY
Vol. 277, No. 23, Issue of June 7, pp. 20854–20861, 2002

Printed in U.S.A.

High Resolution X-ray Structure of Galactose Mutarotase from *Lactococcus lactis**

Received for publication, February 11, 2002, and in revised form, March 16, 2002
Published, JBC Papers in Press, March 20, 2002, DOI 10.1074/jbc.M201415200

James B. Thoden‡ and Hazel M. Holden

From the Department of Biochemistry, University of Wisconsin, Madison, Wisconsin 53706

Galactose mutarotase plays a key role in normal galactose metabolism by catalyzing the interconversion of β-D-galactose and α-D-galactose. Here we describe the three-dimensional architecture of galactose mutarotase from *Lactococcus lactis* determined to 1.9-Å resolution. Each subunit of the dimeric enzyme displays a distinctive β-sandwich motif. This tertiary structural element was first identified in β-galactosidase and subsequently observed in copper amine oxidase, hyaluronate lyase, chondroitinase, and maltose phosphorylase. Two cis-peptides are found in each subunit, namely Pro^{67} and Lys^{136}. The active site is positioned in a rather open cleft, and the electron density corresponding to the bound galactose unequivocally demonstrates that both anomers of the substrate are present in the crystalline enzyme. Those residues responsible for anchoring the sugar to the protein include Arg^{71}, His^{96}, His^{170}, Asp^{243}, and Glu^{304}. Both His^{96} and His^{170} are strictly conserved among mutarotase amino acid sequences determined thus far. The imidazole nitrogens of these residues are located within hydrogen bonding distance to the C-5 oxygen of galactose. Strikingly, the carboxylate group of Glu^{304} is situated at ~2.7 Å from the 1′-hydroxyl group of galactose, thereby suggesting its possible role as a general acid/base group.

In most organisms, the conversion of β-D-galactose to glucose 1-phosphate occurs through the action of four enzymes belonging to the Leloir pathway. As indicated in Scheme 1, galactose mutarotase catalyzes the first step of this pathway, namely the conversion of β-D-galactose to α-D-galactose (1). While mutarotase activity was first reported in *Escherichia coli* in 1965 (2), until recently it was commonly believed that intracellular mutarotation of β-D-galactose occurred spontaneously and that this enzyme was not part of the Leloir pathway (1). Since 1986, however, genes encoding enzymes with mutarotase activities have been identified in *Acinetobacter calcoaceticus* (3), *Streptococcus thermophilus* (4), *Lactobacillus helveticus* (5), *Haemophilus influenzae* (6), *E. coli* (1) and *Lactococcus lactis* (7), for example. A survey of the SWISS-PROT data bank reveals ~45 amino acid sequences that probably code for mutarotases. These enzymes have typical lengths of between 325 and 390 residues. Amino acid sequence alignments demonstrate that these proteins are homologous with sequence identities ranging from 26 to 38% and sequence similarities ranging from 45 to 58%. Interestingly, however, the mutarotases show no amino acid sequence similarities to other proteins in the data bank.

Within recent years, the enzyme from *E. coli* has been the subject of various biochemical analyses (1, 8, 9). These investigations have revealed that the enzyme requires neither bound metal ions nor cofactors for activity and that it functions as a monomer. A possible catalytic mechanism, first suggested by Hucho and Wallenfels (9), involves the abstraction of a proton from the 1′-hydroxyl group of the sugar by an enzymatic base while a side chain acidic group donates a proton to the C-5 oxygen. This results in cleavage of the ring, thereby yielding the open chain aldehyde. Rotation about the C-1–C-2 bond, followed by abstraction of the proton on the C-5 oxygen and donation of a proton back to the C-1 hydroxyl oxygen leads to product formation. Well over 30 years ago, experiments designed to investigate the dependence of mutarotase activity as a function of pH demonstrated the importance of two functional groups, one serving a catalytic role with a pK of 5.5 and the other functioning in substrate binding with a pK of 7.6 (9). Recent site-directed mutagenesis experiments targeted at two conserved histidine residues, namely His^{104} and His^{175} in *E. coli*, suggest that these residues play critical roles in the reaction mechanism (8). The possible roles of either aspartates or glutamates in the reaction mechanism of galactose mutarotase were investigated by treating the enzyme with 1-ethyl-3-(3-dimethylaminopropyl)carbodiimide hydrochloride or aminomethanesulfonic acid (8). These experiments demonstrated a complete loss of enzymatic activity, but the apparent failure to identify a conserved glutamate or aspartate in the amino acid sequence alignments ruled out the possibility of their roles as catalytic bases.

Despite the fact that mutarotases have been isolated from various sources including mammals, plants, fungi, and bacteria, there is still no information available regarding their overall three-dimensional architectures. Here we describe the cloning, expression, purification, and high resolution x-ray crystallographic analysis of galactose mutarotase from *L. lactis*, both in its apo form to 1.9-Å resolution and complexed with α,β-D-galactose to 1.95-Å resolution. This enzyme was selected for study in part because it is believed to play a key role in linking xylan degradation to xylose metabolism (7). Indeed, xylan degradation represents one-third of all renewable carbon (10). The *L. lactis* enzyme contains 339 amino acid residues per subunit. From this investigation, it is now known that the enzyme from *L. lactis* is dimeric rather than monomeric and that its three-dimensional motif is similar to those observed in copper amine oxidase (11), hyaluronate lyase (12), chondroiti-

* This work was supported in part by National Institutes of Health Grant DK47814 (to H. M. H.). The costs of publication of this article were defrayed in part by the payment of page charges. This article must therefore be hereby marked "*advertisement*" in accordance with 18 U.S.C. Section 1734 solely to indicate this fact.

The atomic coordinates and structure factors (code 1L7J and 1L7K) have been deposited in the Protein Data Bank, Research Collaboratory for Structural Bioinformatics, Rutgers University, New Brunswick, NJ (http://www.rcsb.org/).

‡ To whom correspondence should be addressed: Dept. of Biochemistry, University of Wisconsin, 433 Babcock Dr., Madison, WI 53706. Tel.: 608-262-0529; Fax: 608-262-1319; E-mail: JBThoden@facstaff.wisc.edu.

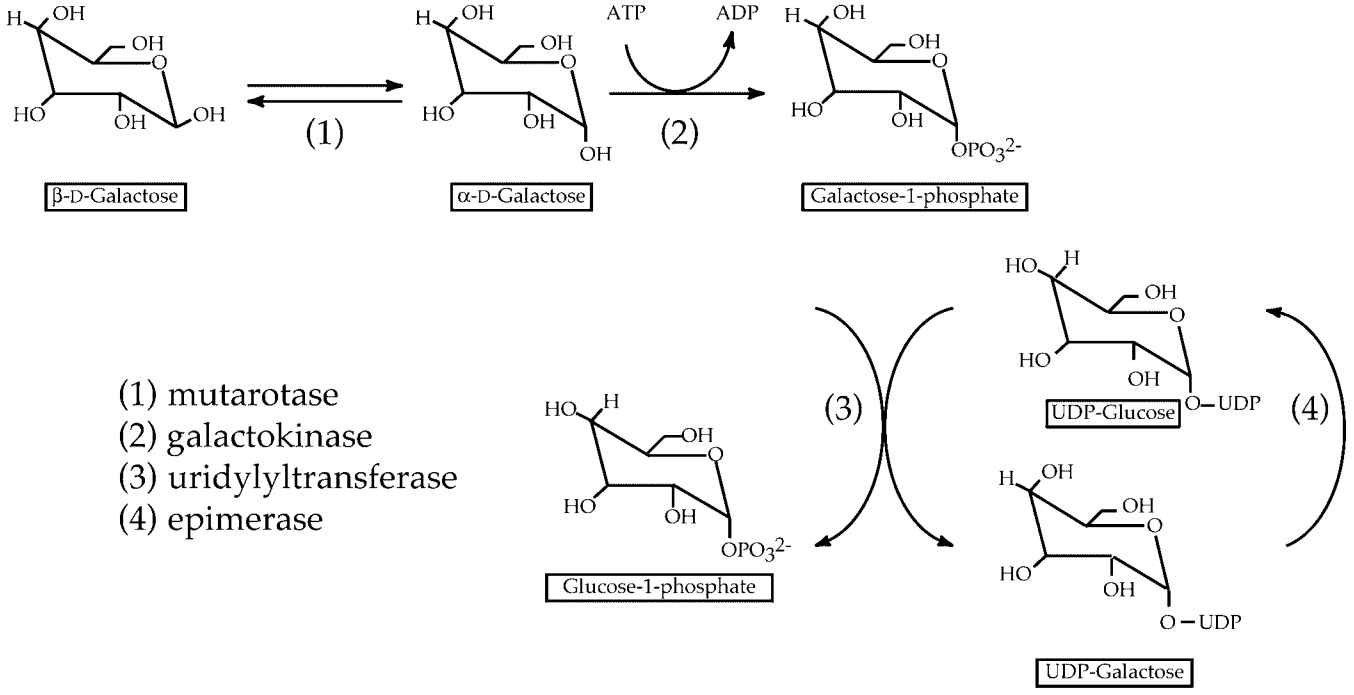

SCHEME 1

TABLE I
X-ray data collection statistics

Data set	Resolution	Independent reflections	Completeness	Redundancy	Avg *I*/Avg $\sigma(I)$	R_{sym}[a]
	A		%			
Native 1	30.0–2.60	20,250	95.8	1.7	4.4	9.8
	2.72–2.60[b]	1961	85.9	1.2	1.8	23.3
Mercury	30.0–2.60	21,877	97.4	2.8	4.7	9.9
	2.72–2.60	2310	89.9	1.6	1.9	23.1
Gold	30.0–2.60	21,015	95.1	2.5	4.4	9.9
	2.72–2.60	2153	87.0	1.5	1.8	23.4
Platinum	30.0–2.80	15,146	90.2	1.9	4.2	10.1
	2.93–2.80	847	51.4	1.1	1.7	20.9
Native 2	30.0–1.90	49,650	92.6	3.2	12.2	8.1
	1.99–1.90	5683	86.7	2.6	4.5	18.0
Galactose	30.0–1.95	51,652	94.2	2.9	12.0	6.3
	2.03–1.95	5042	74.2	1.8	3.4	22.5

[a] $R_{sym} = (\Sigma \mid I - \bar{I} \mid / \Sigma I) \times 100$.
[b] Statistics for the highest resolution bin.

TABLE II
Relevant refinement statistics

Complex	Native	Galactose
Resolution limits (Å)	30.0–1.90	30.0–1.95
R-factor (overall)[a] (%/no. rflns)	19.7/49650	16.1/51652
R-factor (working) (%/no. rflns)	18.9/44968	15.7/46551
R-factor (free) (%/no. rflns)	26.7/5090	21.6/5081
No. of protein atoms	5295[b]	5381[c]
No. of heteroatoms	770 (waters)	479[d]
Bond lengths (Å)	0.014	0.013
Bond angles (degrees)	2.45	2.10
Trigonal planes (Å)	0.006	0.006
General planes (Å)	0.015	0.012
Torsional angles (degrees)[e]	20.5	18.8

[a] *R*-factor = $(\Sigma \mid F_o - F_c \mid / \Sigma \mid F_o \mid) \times 100$, where F_o is the observed structure-factor amplitude and F_c is the calculated structure-factor amplitude.
[b] These include multiple conformations for Leu[46], Lys[52], and Ser[193] in subunit 1 and Ser[140] and Asp[285] in subunit II.
[c] These include multiple conformations for Lys[73] and Ser[140] in subunit I and Lys[82] and Glu[326] in subunit II.
[d] These include two α,β-D-galactose moieties, one sodium ion, and 452 waters.
[e] The torsional angles were not restrained during the refinement.

nase (13), β-galactosidase (14), and maltose phosphorylase (15). Additionally, this investigation has revealed the manner in which the two conserved histidines, His[96] and His[170], interact with the sugar substrate.

EXPERIMENTAL PROCEDURES

Purification of Genomic DNA—5-ml cultures of *L. lactis* var. *lactis* were grown overnight at 30 °C in LB media. The cells were harvested by centrifugation at 3000 × *g* for 15 min, and the cell pellet was suspended in 1 ml water and spun down in a microcentrifuge tube at 14,000 × *g* for 3 min. The washed cell pellet was suspended in 500 μl of lysis buffer, which consisted of 100 mM Tris (pH 8.0), 50 mM EDTA, and 1% SDS. Subsequently, 1.25 ml of 0.3-mm glass beads were added to the suspension, which was vortexed for 2 min to disrupt the cells. The cellular debris was removed by centrifugation, and 275 μl of 7.0 M ammonium acetate (pH 7.0) were added, followed by incubation for 5 min at 65 °C and then 5 min at 0 °C. 500 μl of chloroform were added, and the mixture was vortexed and then spun at 14,000 × *g* for 2 min. The aqueous phase was removed, and the genomic DNA was precipitated by the addition of 1 ml of isopropyl alcohol. After incubation for 5 min at room temperature, the genomic DNA was recovered by centrifugation at 14,000 × *g* for 5 min, washed with 500 μl of 70% ethanol, and, after drying, suspended in 75 μl of water.

Cloning of the Galactose Mutarotase Gene—The *L. lactis* var. *lactis* galactose mutarotase gene was amplified from genomic DNA using the forward primer 5′-CCCACATGTCTATTAAAATAAGAGATTTTGGC-3′ and the reverse primer 5′-CCGCTCGAGTTTTGTATGCAAGCTGTA-AAT-3′. The forward primer was designed with an *Afl*III restriction site at the start codon (which led to the mutation of Glu-2 to serine) and the reverse primer with a *Xho*I restriction site after the codon for the C-terminal lysine residue. This construct allowed for insertion of the PCR gene product into pET28b(+) (Novagen) with a C-terminal His_6 tag. The PCR amplification was performed via the following protocol with Platinum *Pfx* DNA polymerase (Invitrogen): cycle 1, 94 °C for 3 min; cycles 2–31, 94 °C for 1 min, 45 °C for 1.5 min, 72 °C for 2 min (per cycle); and, finally, cycle 32, 72 °C for 10 min. The PCR product was purified with the QIAquick PCR Purification Kit (Qiagen Inc.). The uncut PCR product was subjected to A-tailing modification of the 3′-ends (70 °C for 30 min) using Platinum *Taq* polymerase (Invitrogen). The modified PCR product was then ligated into pGEM-T vector (Promega) and used to transform *E. coli* DH5α cells. These cells were then tested for the PCR insert via blue:white screening of the transformants. Positive (white) colonies were selected and grown overnight in 5-ml cultures of LB media supplemented with ampicillin, and plasmids were purified with the QIAprep Spin Miniprep Kit (Qiagen Inc.). The galactose mutarotase gene was subsequently excised from the pGEM-T Vector construct by digestion with *Afl*III and *Xho*I and ligated into pET28b(+) that had been digested with *Nco*I and *Xho*I. The pET28b(+)-galactose mutarotase vector was used to transform *E. coli* DH5α cells, which were then plated onto LB media plates, supplemented with kanamycin. Ten single colonies were selected, cultured, and mini-prepped for plasmids. The plasmids were first screened by digestion with *Nco*I and *Xho*I. Three plasmids giving positive results (loss of the *Nco*I restriction site) were then sequenced with the ABI PRISM™ Big Dye Primer Cycle Sequencing Kit (Applied Biosystems, Inc.) to confirm the sequence of the galactose mutarotase gene.

Protein Expression and Purification—For protein expression, the pET28b(+)-galactose mutarotase plasmid was used to transform *E. coli* Rosetta cells (Novagen). 5-ml cultures were grown in LB media (supplemented with kanamycin and chloramphenicol) for 7 h at 37 °C. 50 μl were then transferred to 250 ml of the supplemented LB media in a 1-liter shaker flask and grown overnight at 37 °C. 10 ml of the overnight culture were transferred into 600 ml of M9 media (supplemented with kanamycin and chloramphenicol) in 2-liter shaker flasks and grown at 37 °C until an optical density of 0.8 was achieved at 600 nm. The temperature of the incubator was lowered to 20 °C, and after 1 h, isopropyl-1-thio-β-D-galactopyranoside was added to a final concentration of 1 mM. Cell growth was allowed to continue at 20 °C for an additional 15 h.

The cells were harvested by centrifugation at 4000 × *g* for 15 min and frozen in liquid nitrogen. 18 g of frozen cells were thawed in 50 ml of lysis buffer consisting of 50 mM NaH_2PO_4, 300 mM NaCl, and 10 mM imidazole (pH 8.0). The thawed cells were placed in an ice bath and disrupted by three rounds of sonication (1-min duration each) separated by 5 min of cooling. Cellular debris was removed by centrifugation at 20,000 × *g* for 25 min. The clarified supernatant was loaded onto a 15-ml Ni^{2+}-nitrilotriacetic acid-agarose column (Qiagen) that had been previously equilibrated with lysis buffer. The column was then washed with 100 ml of lysis buffer followed by 50 ml of a wash buffer containing 50 mM NaH_2PO_4, 300 mM NaCl, and 20 mM imidazole (pH 8.0). The protein was eluted with a gradient of 100 ml of wash buffer and 100 ml of elution buffer containing 50 mM NaH_2PO_4, 300 mM NaCl, and 350 mM imidazole (pH 8.0). Protein containing fractions were pooled based on purity as judged by SDS-PAGE and dialyzed against 10 mM HEPES and 200 mM NaCl (pH 7.5). The dialyzed protein was concentrated to 17.5 mg/ml based on the extinction coefficient of 0.8 cm/(mg ml) as calculated by the program Protean (DNASTAR, Inc., Madison, WI).

Enzymatic Assay—The coupled assay described by Gatz *et al.* (3) was used to detect mutarotase activity. Briefly, the reaction mixture consisted of a solution made from 906 μl of 100 mM sodium HEPES (pH 7.5), 30 μl of 100 mM NAD^+, and 14 μl of 2688 units/ml glucose dehydrogenase (Sigma). 50 μl of 33.3 mM α-D-glucose were added, and the absorbance was monitored at 340 nm for 2 min for the determination of the spontaneous mutarotation rate. 5 μl of 17.5 mg/ml galactose mutarotase were then added, and the reaction was monitored for another 5 min. The rate calculated after the addition of the enzyme was corrected by subtracting the spontaneous rate, and from this the specific activity was calculated to be 134 units/mg of enzyme, where 1 unit of mutarotase activity is defined as the amount of enzyme needed to convert 1 μmol of α-D-glucose to β-D-glucose per min. The specific activity for α-D-galactose as a substrate was determined in an analogous manner to be 62 units/mg of protein.

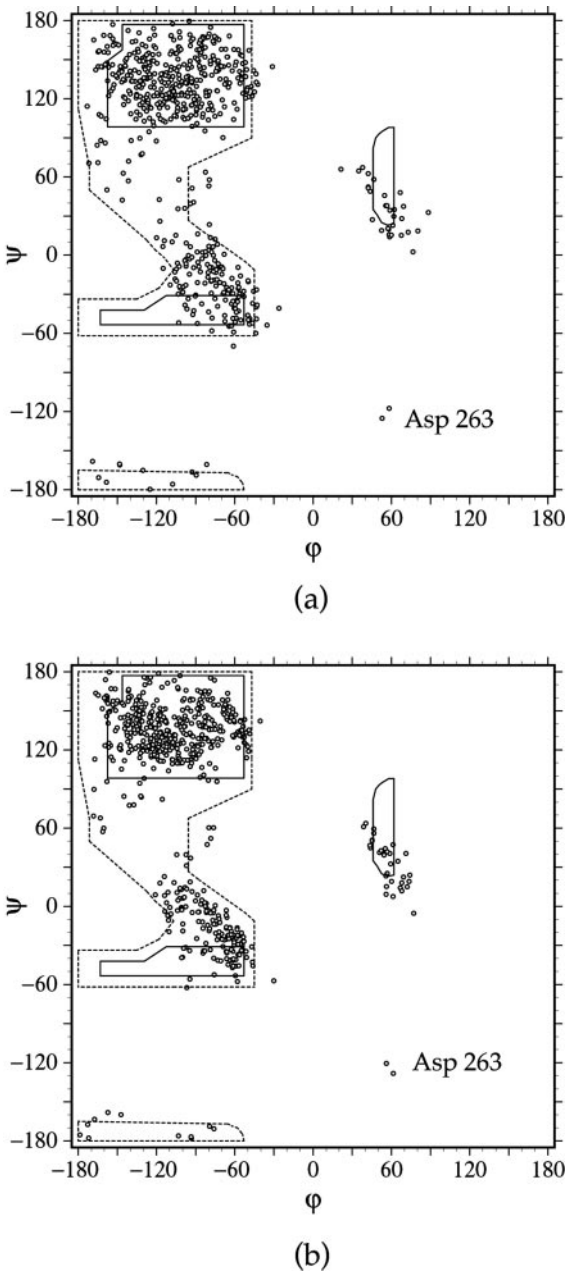

FIG. 1. **Plot of main chain dihedral angles.** Ramachandran plots of all nonglycinyl main chain dihedral angles for the apo form of galactose mutarotase and the complex of the enzyme with galactose are given in *a* and *b*, respectively. Fully allowed ϕ,ψ values are enclosed by *continuous lines*; those only partially allowed are enclosed by *broken lines*.

Crystallization of Galactose Mutarotase—A search for crystallization conditions was conducted utilizing a sparse matrix screen composed of 144 conditions at both room temperature and at 4 °C via the hanging drop method of vapor diffusion. The best crystals were observed growing at 4 °C from poly(ethylene glycol) 5000-*O*-methyl ether (PEG-5000-OMe) at pH 6.0. Large single crystals were subsequently obtained from hanging drops with precipitant solutions of 15–19% PEG-5000-OMe buffered with 100 mM MES (pH 6.0) and enzyme concentrations of 17.5 mg/ml. Crystals achieved maximum dimensions of 0.3 × 0.3 × 0.2 mm in ~1–2 weeks. They belonged to the space group $P2_12_12_1$ with unit cell dimensions of a = 44.8 Å, b = 76.3 Å, and c = 211.1 Å and contained one dimer in the asymmetric unit.

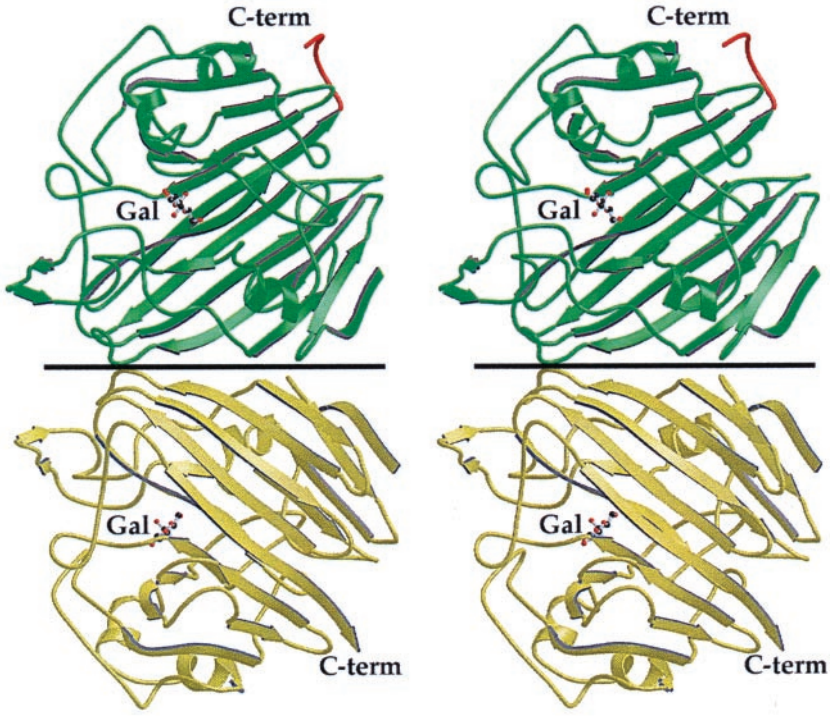

FIG. 2. **Ribbon representation of the galactose mutarotase dimer complexed with α,β-D-galactose.** This *figure* and Figs. 3–7 were prepared with the software package MOLSCRIPT (28). Subunits I and II in the asymmetric unit are *color-coded* in *yellow* and *green*, respectively. The His tag tail, visible at the C terminus of subunit II, is shown in *red*. The galactose moieties are displayed in ball-and-stick representations. The molecular dyad relating the two subunits in the dimer lies in the *plane* of the *figure* as indicated by the *thin black line*.

Structural Analysis of Apo Galactose Mutarotase—An initial x-ray data set was collected to 2.6-Å resolution at 4 °C with a Bruker HISTAR area detector system equipped with Göbel focusing optics. The x-ray source was CuKα radiation from a Rigaku RU200 x-ray generator operated at 50 kV and 90 mA. The x-ray data were processed with SAINT (Bruker AXS, Inc.) and internally scaled with XSCALIBRE.[2] X-ray data collection statistics are presented in Table I.

Three isomorphous heavy atom derivatives were prepared by soaking native crystals in either 2 mM methylmercury acetate for 1 day, 25 mM gold thioglucose for 1 day, or 7 mM K_2PtCl_4 for 7 days. X-ray data were collected for these heavy atom derivatives to 2.6-, 2.6-, and 2.8-Å resolution, respectively. The *R*-factors between the native and mercury, gold, and platinum derivative data sets were 15.2, 12.1, and 15.9%, respectively (where $R = \Sigma \mid F_N - F_h \mid / \Sigma \mid F_N \mid \times 100$, F_N is the native structure factor amplitude, and F_h is the heavy atom derivative structure factor amplitude). Heavy atom binding sites (two per derivative) were determined with SOLVE (17). The positions, occupancies, and temperature factors of these sites were refined with SOLVE, yielding an overall figure-of-merit of 0.38 and phasing powers of 0.96, 0.68, and 0.82, respectively, for the three derivatives. Protein phases were calculated to 2.6-Å resolution with SOLVE. The rotational and translational matrices relating the two subunits in the asymmetric unit were determined with the program MUNCHKINS (18) based on the positions of the two mercury atom binding sites. These matrices were employed for cyclical averaging with the solvent flattening software, DM (19), to give a figure-of-merit of 0.82 for the averaged electron density map. 85% of the residues were built into the averaged electron density map using TURBO (20). The model was then expanded back into the crystallographic cell and refined with TNT (21). The resulting electron density maps calculated with coefficients of the form $2F_o - F_c$ or $F_o - F_c$ were then averaged with the program AVE in the RAVE suite of programs (22, 23) and allowed for the placement of the remainder of the amino acid residues.

High Resolution X-ray Data Collection and Least-squares Refinement—Galactose mutarotase crystals were harvested from hanging drop experiments and equilibrated in a synthetic mother liquor composed of 20% PEG-5000-OMe, 200 mM NaCl, and 100 mM MES (pH 6.0). They were then serially transferred to a cryoprotectant solution containing 25% PEG-5000-OMe, 400 mM NaCl, 17.5% ethylene glycol, and 100 mM MES (pH 6.0). The crystals were suspended in a loop of 20-μm nylon and flash-frozen in a stream of nitrogen gas. Unit cell dimensions changed to $a = 42.5$ Å, $b = 76.1$ Å, and $c = 206.8$ Å upon cooling to 120 K. A native x-ray data set was collected to 1.9-Å resolution and processed and scaled as previously described. This structure was solved via molecular replacement with the program AMORE (24) and employing as the search model the partially refined structure determined at 2.6-Å resolution. Initial least-squares refinement to 2.2-Å resolution lowered the *R*-factor to 28.5%. Electron density maps calculated with either ($2F_o - F_c$) or ($F_o - F_c$) coefficients were subjected to molecular averaging with AVE. An "averaged" model was built and placed back into the unit cell for further least-squares refinement. Iterative cycles of least-squares refinement and manual model building reduced the *R*-factor to 19.7% for all measured x-ray data from 30.0- to 1.9-Å resolution. Least-squares refinement statistics are presented in Table II.

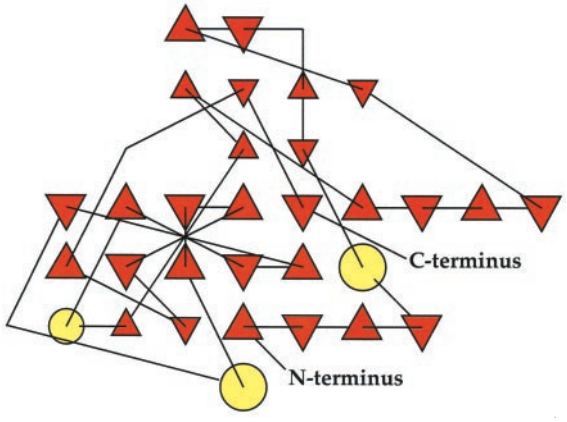

FIG. 3. **Topological arrangement of the secondary structural elements observed in galactose mutarotase.** This figure was graciously prepared by Dr. Ioannis Michalopoulos (Research Fellow in Bioinformatics, School of Biochemistry and Molecular Biology, University of Leeds). *Triangles* indicate β-strands, while *circles* represent α-helical regions.

Structural Analysis of Galactose Mutarotase Complexed with α,β-D-Galactose—Apogalactose mutarotase crystals were harvested from the hanging drop experiments and equilibrated in a synthetic mother liquor composed of 20% PEG-5000-OMe, 200 mM NaCl, 100 mM MES (pH 6.0), and 100 mM α-D-galactose. After equilibration for 24 h at 4 °C, an x-ray data set was collected to 1.95-Å resolution at 4 °C and processed and scaled as previously described. This structure was solved via molecular replacement with the software package AMORE (24) and employing as the search model the x-ray coordinates for the native enzyme. Iterative

[2] I. Rayment and G. Wesenberg, unpublished results.

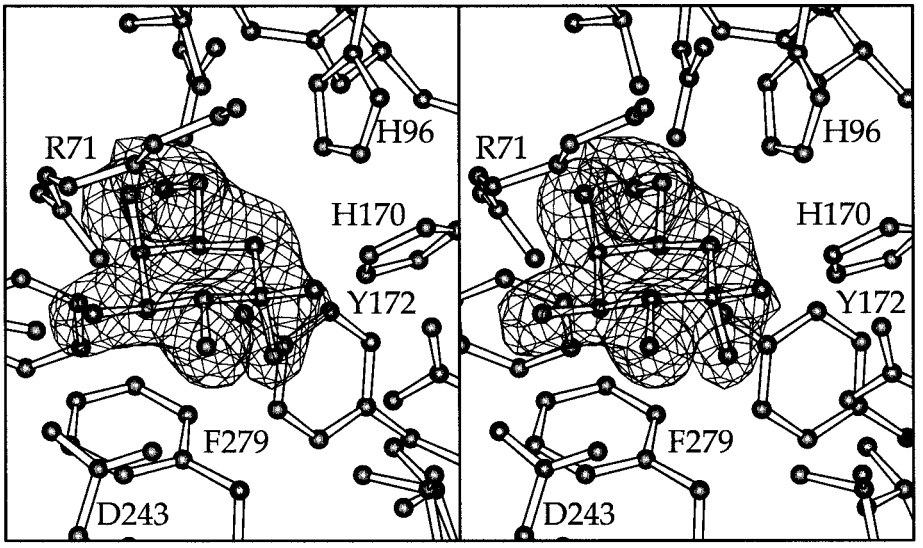

FIG. 4. **Electron density corresponding to galactose bound in the active site of subunit II.** The map shown was calculated with coefficients of the form $(F_o - F_c)$, where F_o was the native structure factor amplitude and F_c was the calculated structure factor amplitude from the model lacking the coordinates for the sugar ligand. The map was contoured at 2.5 σ.

rounds of refinement with TNT and manual manipulation with TURBO reduced the *R*-factor to 16.1% for all observed data from 30.0- to 1.95-Å resolution. Refinement statistics are presented in Table II.

RESULTS AND DISCUSSION

Three-dimensional Structure of the Apo Form of Galactose Mutarotase—The model for the apoenzyme presented here refined to an *R*-factor of 19.7% for all measured x-ray data with excellent overall stereochemistry as indicated in Table II. There are two cis-peptide bonds in each subunit, one at Pro^{67} and the other at Lys^{136}. Pro^{67} is buried and located at ~5.5 Å from the active site His^{96}. In contrast, Lys^{136} is positioned at the subunit:subunit interface. Most of the dihedral angles lie well within the allowed regions of the Ramachandran plot (Fig. 1*a*), with only Asp^{263} adopting torsional angles of $\phi = \sim 59°$ and $\psi = \sim -124°$. Asp^{263} is located in a type II′ turn delineated by Leu^{262} to Thr^{265} and is well removed from both the subunit:subunit interface and the active site. The electron densities corresponding to both subunits are well ordered. Only the electron density for the loop delineated by Asn^{214} to Asp^{216} in subunit I is somewhat weaker than that observed for the rest of the molecule. Each subunit of the apoenzyme extends continuously from Ser^2 to Lys^{339}.

A ribbon representation of the galactose mutarotase dimer is presented in Fig. 2. While the mutarotase isolated from *E. coli* is reported to be monomeric, the packing of the *L. lactis* enzyme in the crystalline lattice suggested a dimeric quaternary structure. Indeed, the buried surface area between the two subunits in the asymmetric unit, based on a probe radius of 1.4 Å, is 1900 $Å^2$ (25). Subsequent ultracentrifugation experiments confirmed the dimeric nature of the galactose mutarotase from *L. lactis*.[3] Each subunit contributes primarily three regions of secondary structure to form the dimeric interface: 1) a type I′ turn defined by Gly^9 and Ser^{12} and connecting the first two β-strands, 2) a type I turn/β-strand motif delineated by Glu^{100} to Tyr^{109}, and 3) a succession of type II, type II, and type I′ turns lying between Asn^{127} and Lys^{136}. The subunit:subunit interface is fairly hydrophilic, with numerous hydrogen bonds between side chains and/or backbone atoms. As an example, the ϵ-amino group of Lys^{105} (subunit I) lies within hydrogen bonding distance to $O^{\delta 1}$ of Asn^{127} and O of Val^{125} (subunit II). In turn, $N^{\delta 2}$ of Asn^{127} (subunit II) lies within hydrogen bonding distance to the carbonyl oxygens of both Glu^{99} and Glu^{100} in subunit I. Numerous water molecules line the subunit:subunit interface. The overall dimensions of the apoenzyme are ~50 × 86 × 83 Å. The structures of the two subunits contained within the asymmetric unit are exceedingly similar such that all of their atoms superimpose with a root mean square deviation of 0.70 Å.

Each monomer, with overall dimensions of 46 × 60 × 52 Å, folds into one domain that is dominated by extensive layers of β-sheet. The three-dimensional architecture of the monomer, which can be aptly described as a β-sandwich, is similar to the 18-stranded, anti-parallel motif observed for domain 5 of β-galactosidase (14). In the galactose mutarotase, there are 28 strands of β-sheet connected by three small α-helices and nine type I, six type I′, nine type II, three type II′, and three type III reverse turns. The strands of β-sheet range in length from 2 to 11 residues. A topological drawing of the three-dimensional architecture of galactose mutarotase is presented in Fig. 3. The N and C termini are located on the same side of the molecule and separated by ~26 Å.

Three-dimensional Structure of Galactose Mutarotase Complexed with α,β-D-Galactose—The quality of the model for galactose mutarotase complexed with α,β-D-galactose is outstanding as indicated by an *R*-factor of 16.1% for all measured x-ray data and overall excellent geometry. A Ramachandran plot for the model is presented in Fig. 1*b*. The two subunits in the asymmetric unit superimpose with root mean square deviations of 0.25 and 0.60 Å for α-carbons and all atoms, respectively. Both the N and C termini are well ordered, and, like the apoenzyme structure, there are no breaks in the polypeptide chains for either subunit. In fact, the His tag at the C terminus of subunit II is completely ordered, adopts an extended conformation, and is involved in crystal contacts. It is located at ~30 Å from the active site.

There are very few structural differences between the apo and sugar-bound forms of the enzyme such that their α-carbon atoms and all atoms superimposed with root mean square deviations of 0.30 and 0.70 Å, respectively. Indeed, the sugar substrate is accommodated within the active site via movement of solvent molecules rather than major perturbations of side chain conformations except for that of Phe^{279}. The aromatic ring of Phe^{279} shifts somewhat to accommodate the 1′-hydroxyl group of galactose in its α-anomeric configuration. The active site of the enzyme is located in a quite wide and shallow cleft, explaining in part the broad specificity of the enzyme toward various sugar substrates. The two active sites in the dimer are separated by ~43 Å.

[3] J. Kim, personal communication.

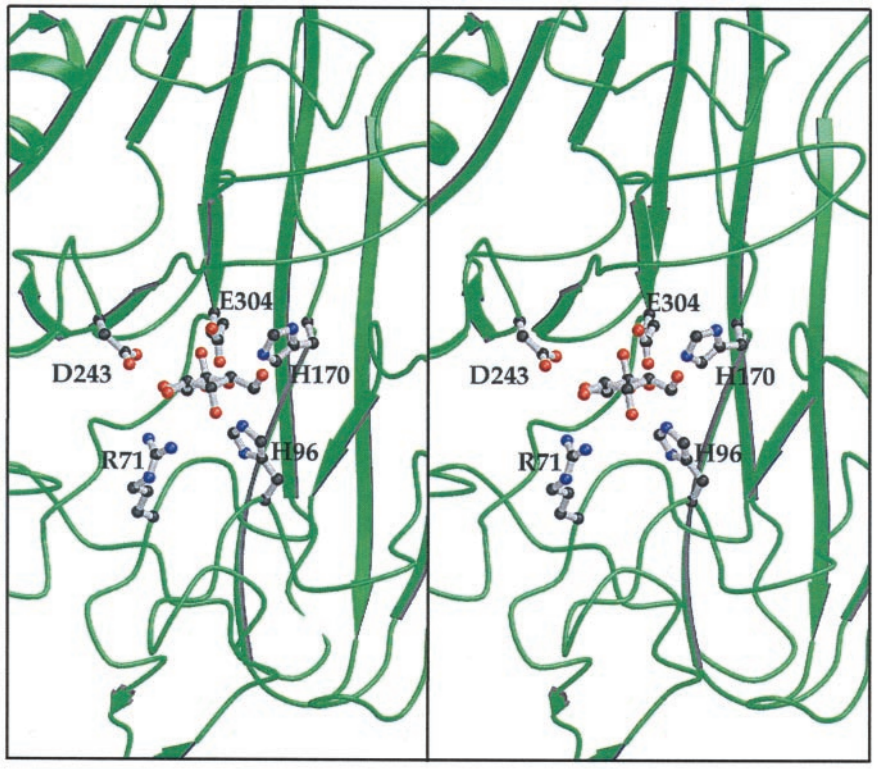

(a)

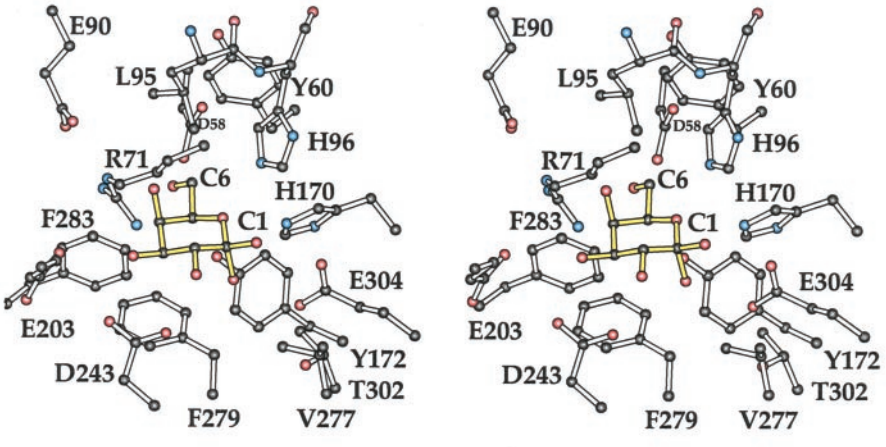

(b)

FIG. 5. **Close-up view of the active site of galactose mutarotase.** Shown in *a* are the key residues responsible for sugar binding in context with secondary structural elements. As can be seen, the cleft responsible for sugar binding is quite wide and close to the surface of the protein. Shown in *b* are those residues located within 5 Å of the galactose molecule. The eight ordered water molecules surrounding the sugar were removed to enhance clarity.

The electron densities corresponding to the bound galactose moieties are well ordered in both subunits. Shown in Fig. 4 is the observed electron density corresponding to the galactose moiety bound in subunit II. As can be seen, the electron density indicates a mixture of both the α- and β-anomers of D-galactose. For model refinement purposes, the occupancies corresponding to the two configurations of the 1′-hydroxyl groups were set to 0.5. In both subunits I and II, the *B*-factors for the 1′-hydroxyl groups in the β-anomeric positions are $\sim$24 Å^2, whereas those for the α-anomeric positions are $\sim$12 Å^2. While caution must be applied in the interpretation of temperature factors, these *B*-values suggest that the two configurations about the anomeric carbon of galactose are not equally distributed in the crystalline enzyme. Interestingly, at equilibrium in aqueous solutions at 40 °C, the percentage of D-galactose in the β-configuration is between 64 and 73% (26). The average *B*-values for all the

galactose atoms are 22.8 and 20.3 Å^2, in subunits I and II, respectively.

A close up view of the active site for subunit II, in the context of secondary structure, is presented in Fig. 5*a*. Key residues involved in sugar binding include Arg^{71}, His^{96}, His^{170}, Asp^{243}, and Glu^{304}. In addition to forming hydrogen bonds with the sugar ligand, the guanidinium group of Arg^{71} also participates in a salt bridge with the carboxylate group of Glu^{90}. Arg^{71} is located in a coil region of secondary structure. His^{96} is positioned in a type I′ turn defined by Leu^{95}–Gly^{98}, whereas His^{170}, Asp^{243}, and Glu^{304} are located on β-strands. Both His^{96} and His^{170}, separated by ~4 Å, are strictly conserved among 34 galactose mutarotase sequences examined in the SWISS-PROT data bank. Additionally, Arg^{71}, Asp^{243}, and Glu^{304} are strictly conserved among 33 of the sequences. In the cases where these residues are not conserved, they are replaced with a histidine, a glutamate, and a glutamine, respectively.

Those amino acid residues lying within 5 Å of galactose are indicated in Fig. 5*b*. Both hydrophobic and hydrophilic side chains contribute to the formation of this sugar-binding region. The bottom part of the binding pocket, as oriented in Fig. 5*b*, is somewhat hydrophobic and lined with three aromatic residues, Tyr^{172}, Phe^{279}, and Phe^{283}. Tyr^{172} is conserved among 33 galactose mutarotases but is replaced with a leucine in one of the sequences. Likewise, the aromatic nature of Phe^{279} is conserved among the mutarotases with four containing phenylalanines at this position and the other 30 containing tyrosines. Two additional hydrophobic residues, Tyr^{60} and Leu^{95}, form the top half of the binding pocket and are not strictly conserved. There are eight water molecules lying within 5 Å of the galactose moiety.

A schematic diagram of the potential hydrogen bonding interactions between the galactose ligand and the protein is shown in Fig. 6. Four water molecules interact with the substrate. One is situated within 2.9 Å of the 6′-hydroxyl group, while the second resides near the 3′-hydroxyl group (2.8 Å). A third water molecule bridges the 2′-hydroxyl group (2.7 Å) and the 1′-hydroxyl group when it is in the β-configuration (3.2 Å). The fourth water lies within 3.1 Å of the 1′-hydroxyl group in the β-configuration. The N$^{\epsilon 2}$ atoms of His^{96} and His^{170} are located within ~3 Å of the C-5 oxygen. Strikingly, the carboxylate group of Glu^{304} is positioned to interact with both the α- and β-anomeric forms of galactose. As indicated in Fig. 6, the carboxylate group of Asp^{243} anchors the 2′- and 3′-hydroxyl groups of galactose to the protein. The guanidinium group of Arg^{71} interacts with both the 3′- and 4′-hydroxyl groups of the sugar.

Relationship of Galactose Mutarotase to Other Known Protein Structures—The successful three-dimensional structural analysis of β-galactosidase from *E. coli* in the laboratory of Dr. Brian Matthews represented both a monumental effort and an x-ray crystallographic milestone (14). The structure of this remarkable enzyme was described in terms of five motifs: domain 1 containing a jelly-roll fold, domains 2 and 4 having immunoglobulin folds, domain 3 composed of an α/β barrel and containing the active site residues, and domain 5, which was likened to a β-sandwich. In 1994, domain 5 was thought to possess a novel architecture. Since that time, additional proteins have been observed to contain this motif including the central domain of copper amine oxidase (11), the C-terminal domain of chondroitinase (13), the C-terminal domain of hyaluronate lyase (12), and the N-terminal domain of maltose phosphorylase (15). A search with the DALI server (27) revealed that, indeed, galactose mutarotase belongs to this growing family of proteins containing a β-sandwich motif. Unlike the other proteins studied thus far, however, the β-sandwich motif constitutes the entire structure of galactose mutarotase. A superposition of domain 5 of β-galactosidase onto the galactose mutarotase subunit is presented in Fig. 7. While there is no sequence homology between these proteins, the overall tertiary structural similarities are striking. None of the active site residues in galactose mutarotase are conserved in domain 5 of β-galactosidase. β-galactosidase catalyzes the hydrolysis of lactose to glucose and β-D-galactose, which is then the substrate for galactose mutarotase. It can be speculated that, perhaps, the ancient β-galactosidase was a bifunctional protein contain-

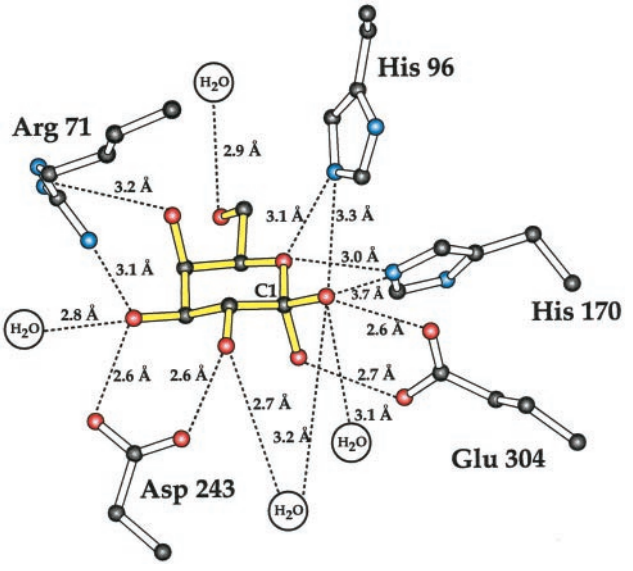

FIG. 6. **Schematic diagram of the hydrogen bonding interactions between the substrate and the enzyme.** The distances quoted are those observed for the galactose moiety when bound in subunit II. The *dashed lines* are meant to indicate possible electrostatic interactions.

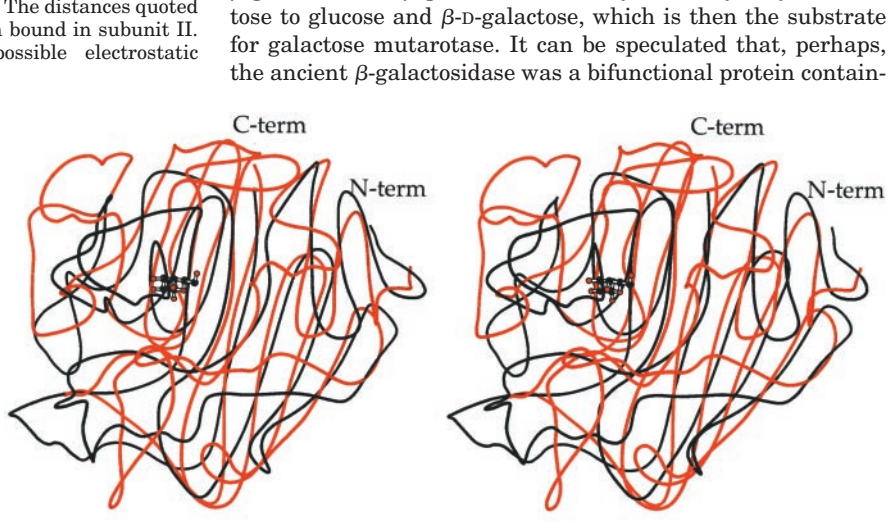

FIG. 7. **Superposition of the polypeptide chains for galactose mutarotase and domain 5 of β-galactosidase.** The α-carbon trace displayed in *black* corresponds to galactose mutarotase, while that depicted in *red* is for residues His^{735} to Lys^{1023} of β-galactosidase. The coordinates for β-galactosidase were obtained from the Protein Data Bank (1BGL).

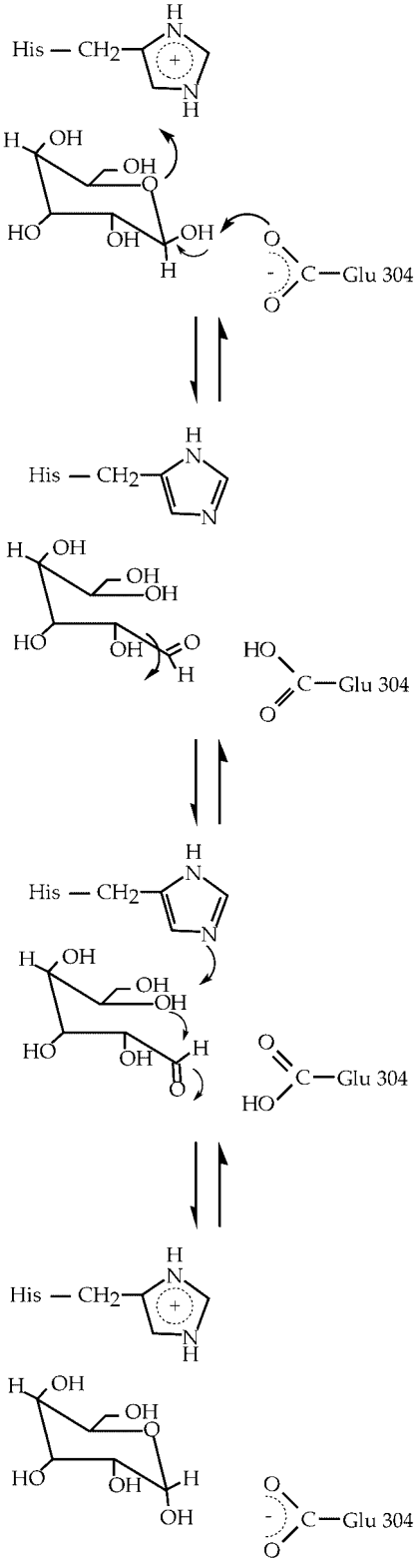

SCHEME 2

ing both β-galactosidase and mutarotase activities. Interestingly, as indicated in the SWISS-PROT data bank, the galactose mutarotase in yeast is part of a larger polypeptide chain containing a sequence coding for UDP-galactose 4-epimerase at its N-terminal region. As such, there is clearly precedence in sugar metabolism for multiple activities contained within one polypeptide chain.

Catalytic Mechanism of Galactose Mutarotase in Context of Structure—The most commonly accepted catalytic mechanism for galactose mutarotase involves three key features: 1) abstraction of the 1′-hydroxyl hydrogen by an enzymatic base, 2) protonation of the C-5 oxygen by an active site acid, and 3) rotation about C-1–C-2 bond when the open chain aldehyde is formed. These features can now be addressed in terms of structure as outlined in Scheme 2. Most likely, Glu^{304}, with its side chain carboxylate group positioned at ~2.7 Å from the 1′-hydroxyl group of galactose, functions to initiate the reaction. Both His^{96} and His^{170} lie within 3 Å of the C-5 oxygen. Either is positioned to serve as the active site acid required to protonate the C-5 oxygen, and it is not clear from the present structure which one serves in such capacity. From the recent and insightful site-directed mutagenesis experiments conducted on the *E. coli* galactose mutarotase, it is known that mutations of either of these histidines result in sharp decreases in enzymatic activities (8). Indeed, for the H104Q mutant protein (corresponding to His^{96} in the *L. lactis* enzyme), a 4000-fold decrease in k_{cat}/K_m was observed as compared with the native enzyme. Additionally, the catalytic activity of the H175A mutant protein of the *E. coli* mutarotase (corresponding to His^{170} in the *L. lactis* enzyme) was too low to measure. Thus, it might be speculated that His^{170} functions as the catalytic acid in the *L. lactis* galactose mutarotase. Experiments designed to further address the roles of Glu^{304}, His^{96}, and His^{170} in the catalytic mechanism of galactose mutarotase are in progress.

Acknowledgments—We thank Dr. Frank M. Raushel for critically reading the manuscript. We also thank Dr. John Lindquist (Department of Bacteriology, University of Wisconsin) for supplying *L. lactis* var. *lactis* cell stock.

REFERENCES

1. Bouffard, G. G., Rudd, K. E., and Adhya, S. L. (1994) *J. Mol. Biol.* **244,** 269–278
2. Wallenfels, K., Hucho, F., and Herrmann, K. (1965) *Biochem. Z.* **343,** 307–325
3. Gatz, C., Altschmied, J., and Hillen, W. (1986) *J. Bacteriol.* **168,** 31–39
4. Poolman, B., Royer, T. J., Mainzer, S. E., and Schmidt, B. F. (1990) *J. Bacteriol.* **172,** 4037–4047
5. Mollet, B., and Pilloud, N. (1991) *J. Bacteriol.* **173,** 4464–4473
6. Maskell, D. J., Szabo, M. J., Deadman, M. E., and Moxon, E. R. (1992) *Mol. Microbiol.* **6,** 3051–3063
7. Erlandson, K. A., Delamarre, S. C., and Batt, C. A. (2001) *Appl. Environ. Microbiol.* **67,** 1445–1452
8. Beebe, J. A., and Frey, P. A. (1998) *Biochemistry* **37,** 14989–14997
9. Hucho, F., and Wallenfels, K. (1971) *Eur. J. Biochem.* **23,** 489–496
10. Prade, R. A. (1996) *Biotechnol. Genet. Eng. Rev.* **13,** 101–131
11. Parsons, M. R., Convery, M. A., Wilmot, C. M., Yadav, K. D., Blakely, V., Corner, A. S., Phillips, S. E., McPherson, M. J., and Knowles, P. F. (1995) *Structure* **3,** 1171–1184
12. Li, S., Kelly, S. J., Lamani, E., Ferraroni, M., and Jedrzejas, M. J. (2000) *EMBO J.* **19,** 1228–1240
13. Féthière, J., Eggimann, B., and Cygler, M. (1999) *J. Mol. Biol.* **288,** 635–647
14. Jacobson, R. H., Zhang, X. J., DuBose, R. F., and Matthews, B. W. (1994) *Nature* **369,** 761–766
15. Egloff, M.-P., Uppenberg, J., Haalck, L., and Van Tilbeurgh, H. (2001) *Structure* **9,** 689–697
16. Gatz, C., Altschmied, J., and Hillen, W. (1986) *J. Bacteriol.* **168,** 31–39
17. Terwilliger, T. C., and Berendzen, J. (1999) *Acta Crystallogr. Sect. D* **55**, 849–861
18. Rypniewski, W. R., Breiter, D. R., Benning, M. M., Wesenberg, G., Oh, B.-H., Markley, J. L., Rayment, I., and Holden, H. M. (1991) *Biochemistry* **30,** 4126–4131
19. Cowtan, K., and Main, P. (1998) *Acta Crystallogr. Sect. D* **54**, 487–493
20. Roussel, A., and Cambillau, C. (1991) in *Silicon Graphics Geometry Partners Directory*, Silicon Graphics, Mountain View, CA
21. Tronrud, D. E., Ten Eyck, L. F., and Matthews, B. W. (1987) *Acta Crystallogr. Sect. A.* **43,** 489–501
22. Jones, T. A. (1992) in *Molecular Replacement* (Dodson, E. J., Gover, S., and Wolf, W., eds) pp. 91–105, SERC Daresbury Laboratory, Warrington, UK
23. Kleywegt, G. J., and Jones, T. A. (1994) in *From First Map to Final Model* (Bailey, S., Hubbard, R., and Waller, D., eds) pp. 59–66, SERC Daresbury Laboratory, Warrington, UK
24. Navaza, J. (1994) *Acta Crystallogr. Sect. A* **50,** 157–163
25. Zhang, X.-J., and Matthews, B. W. (1995) *J. Appl. Crystallogr.* **28,** 624–630
26. Loudon, G. M. (1998) in *Organic Chemistry*, p. 1209, Benjamin/Cummings Publishing Co., Inc., Menlo Park, CA
27. Holm, L., and Sander, C. (1993) *J. Mol. Biol.* **233,** 123–138
28. Kraulis, P. J. (1991) *J. Appl. Crystallogr.* **24,** 946–950